J Arid Land (2025) 17(8): 1084–1102
doi: 10.1007/s40333-025-0027-5; CSTR: 32276.14.JAL.02500275

Science Press Springer-Verlag

Probability and spatiotemporal dynamics of active fire occurrence in Inner Mongolia, China from 2000 to 2022

JIA Xu[1], WEI Baocheng[2,3*], ZHANG Zhijie[4], CHEN Lulu[2], LIU Mengna[2], ZHAO Yiming[2], WANG Jing[1]

[1] College of Resources and Environmental Economics, Inner Mongolia University of Finance and Economics, Hohhot 010051, China;
[2] College of Geographical Science, Inner Mongolia Normal University, Hohhot 010022, China;
[3] Key Laboratory of Mongolian Plateau's Climate System at Universities of Inner Mongolia Autonomous Region, Inner Mongolia Normal University, Hohhot 010022, China;
[4] Hohhot Meteorological Observatory, Hohhot 010020, China

Abstract: Fires are one of the most destructive natural disasters and have serious long-term effects on the environment, economy, and human health. In Inner Mongolia Autonomous Region, China, frequent fire disturbance occurs due to the intensification of climate change and human activities. It is crucial to understand the fire regime and estimate the probability of regional fire occurrence and reducing fire losses. However, most studies have primarily focused on the dynamic changes, probability of occurrence, and driving mechanisms of wildfires in the grassland and forest land ecosystems in Inner Mongolia, while insufficient research has been conducted on the spatiotemporal variations in active fires and their impact on the wildfire risk in forest land and grassland. Therefore, in this study, we analyzed the active fire regime based on Moderate Resolution Imaging Spectroradiometer (MODIS) thermal anomalies and burned area products from 2000 to 2022. Combined with climate, topographic, landscape, anthropogenic, and vegetation datasets, logistic regression (LR), support vector machine (SVM), random forest (RF), and convolutional neural network (CNN) models were chosen to estimate the probability of active fire occurrence at the seasonal timescale. The results revealed that: (1) a total of 100,343 active fires occurred in Inner Mongolia and the burned area reached 6.59×10^4 km^2. The number of ignition point exhibited a significant increasing trend, while the burned area exhibited a nonsignificant decreasing trend; (2) four active fire belts were detected, namely, the Hetao-Tumochuan Plain fire belt, Xiliao River Plain fire belt, Songnen Plain fire belt, and Hailar River Eroded Plain fire belt. The centroid of the active fires has shifted 456.4 km toward the southwest; (3) RF model achieved the highest accuracy in estimating the probability of active fire occurrence, followed by CNN, and LR and SVM models had lower accuracies; and (4) the distribution of the high and extremely high fire risk areas largely aligned with the four fire belts. The probability of active fire occurrence was the highest in spring, followed by that in autumn, and it gradually decreased in summer and winter. Our results revealed active fires migrated to the southwest and ignition sources increased, despite reduction of the burned area was not significant. The RF model outperformed the other models in predicting the probability of active fire occurrence. These findings contribute to future fire prevention and prediction in Inner Mongolia.

Keywords: active fire regime; probability prediction; machine learning; Moderate Resolution Imaging Spectroradiometer (MODIS); random forest model

*Corresponding author: WEI Baocheng (E-mail: nsdwbc@126.com)
Received 2025-03-01; revised 2025-06-10; accepted 2025-07-01

Citation: JIA Xu, WEI Baocheng, ZHANG Zhijie, CHEN Lulu, LIU Mengna, ZHAO Yiming, WANG Jing. 2025. Probability and spatiotemporal dynamics of active fire occurrence in Inner Mongolia, China from 2000 to 2022. Journal of Arid Land, 17(8): 1084–1102. https://doi.org/10.1007/s40333-025-0027-5; https://cstr.cn/32276.14.JAL.02500275

1 Introduction

Active fire refers to real-time fire information captured by satellites and encompasses various types of fires such as vegetation fires, farmland fires, urban fires, and volcanic fires (Zheng et al., 2024). Active fires, as one of the most important natural disturbance factors in flammable ecosystem, have a significant impact on the vegetation structure and function, as well as the exchange and feedback of energy between land surface and atmosphere (Pausas and Keeley, 2021; Haas et al., 2022; McNorton and Di Giuseppe, 2024). Over the past several years, the frequency and scale of active fires have significantly increased due to the intensification of human activities and the frequent occurrence of extreme climate events (Aldersley et al., 2011; Ellis et al., 2021). In addition, the increase in fire incidents poses serious threats to human health, air quality, and global climate change (Kiely et al., 2024; MacCarthy et al., 2024). The recently released "2023–2024 Global Wildfire Report" indicates that unprecedented fire activity has occurred in multiple areas during the global fire season (Jones et al., 2024). For example, there was a historic record for fire extent in Canada in 2023, with a burned area of 15×10^6 hm^2 (Jain et al., 2024). The carbon emissions from global fires were 16.00% above the average level. Therefore, it is crucial to research fire regime and develop reliable fire risk estimation models to effectively prevent and control fires, enhance fire warning capabilities, and reduce environmental and socio-economic losses.

Long-term ground observations and remote sensing monitoring are primary technical methods used in fire research (Wang et al., 2022; Zhai et al., 2022; Touge et al., 2024). Ground observation data clearly record information such as the location, ignition time, burned area, and causes of the fire (Zhang et al., 2024c). However, the high cost and limited coverage of ground observations have become increasingly apparent under the increasing frequency of fires and gradual expansion of the fire area (Liu et al., 2022). Thermal infrared sensors are highly sensitive to surface thermal anomalies and can detect fire points that are smaller than the spatial resolution of satellites, making them a powerful tool for fire monitoring (Chao et al., 2020; Qin et al., 2020).

Moderate Resolution Imaging Spectroradiometer (MODIS) datasets have been used to perform research on active fires (Duan et al., 2024; Vouzoglanis et al., 2024). Over the past decade, relevant researches have been rapidly conducted in China such as fire detection, burned area mapping, damage assessment, biomass burning estimation, and post-fire vegetation recovery monitoring. Moreover, climate change and human activities have exacerbated the frequency and intensity of natural fires, especially in arid, semi-arid, and semi-humid areas (Qarallah et al., 2022; Liu et al., 2023b). In these areas, such as Inner Mongolia Autonomous Region, the increasing frequency and spread of fires have emerged as a significant threat to the ecological environment (Jia et al., 2019; Chang et al., 2023; Zhang et al., 2024d). However, research on the fire regime based on large-scale remote sensing monitoring in these areas is still limited.

It is necessary to develop a fire risk estimation model to enhance fire prevention and management. Statistical linear models such as geographically weighted regression, logistic regression, and linear regression are among the commonly used methods (Milanović et al., 2020; Monjaras-Vega et al., 2020). However, fire occurrence is a typical nonlinear process, and the fire regime is the result of interactions among various factors, including climatic conditions, fuel characteristics, topography, landscape, and human activities (Chen et al., 2023). To overcome this limitation, machine learning models such as random forest, support vector machines, and deep learning models have become popular for estimating fire risk in recent years (Elia et al., 2020; Pang et al., 2022; Belarbi et al., 2024). However, it should be noted that the accuracy of different fire risk estimation models varies significantly, as the driving factors chosen for fire risk analysis differ across areas. In most studies, the explanatory variables driving fire occurrences were analyzed at the annual scale, which made the performance comparison of fire risk models across

different areas less comparable.

Inner Mongolia is located in the interior of the Eurasian continent, and the majority of its land area is covered by natural vegetation (Chen et al., 2022). This area experiences frequent forest and grassland fires during spring and autumn seasons, influenced by the temperate continental monsoon climate and human activities (Zhang et al., 2025). Suitable temperatures and ample precipitation in this area provide favorable water-thermal conditions for vegetation growth in summer. However, rapid wilting of the vegetation generates a large amount of litter in autumn, providing a rich material foundation for the occurrence of fire (Chao et al., 2023). Moreover, frequent occurrence of extreme weather events such as droughts and strong winds from autumn to spring significantly accelerates the risk of fire occurrence, making it easier for fires to spread from one area to another and increasing the extent of their spread (Sun et al., 2021). Human activities such as agricultural production, grazing, and straw burning are also significant factors that trigger regional fires (Li et al., 2017). Extensive researches in this area were conducted on the spatiotemporal dynamics, occurrence risk, and driving mechanisms of wildfires (Chang et al., 2023; Li et al., 2024; Zhang et al., 2024b). However, most studies have overlooked the spatiotemporal variations in farmland fires closely related to human activities and their impact on the wildfire risk in forests and grasslands. For example, Zhang et al. (2024c) pointed out that agricultural fires, such as the burning of straw and discarded plastic film, were significant anthropogenic sources triggering forest fires. Additionally, statistical and machine learning methods have commonly been used in estimating fire occurrence risks, while deep learning methods have primarily been applied for fire detection in small areas, and their potential for estimating fire occurrence risks still requires further validation over large areas.

Therefore, taking Inner Mongolia in China as an example, we utilized MODIS active fire monitoring data from 2000 to 2022 to analyze the fire regime. On this basis, combined with various environmental variables, four predictive models were selected to estimate the probability of active fire occurrence at the seasonal scale. The objectives of this study were: (1) to reveal the evolution process of active fire regime; (2) to assess the probability of active fire occurrence based on four predictive models, and (3) to choose the optimal model for mapping the probability of active fire occurrence at the seasonal and annual scales.

2 Materials and methods

2.1 Study area

Inner Mongolia is located between 37°24′–53°23′N and 97°12′–126°04′E with an area of 1.18×10^6 km^2. The study area has a temperate continental monsoon climate. Annual average temperature ranges from –3.7°C to 11.2°C, and increases from northeast to southeast and southwest. Frequent droughts and strong winds occur in spring. In summer, most areas experience a mild climate with few hot days. Temperature rapidly drops in autumn and winter is long and harsh (Ren et al., 2022). Average annual precipitation is 350–400 mm, which concentrates in summer and decreases from northeast to southwest. Frost-free period lasts for 50–150 d. Topography is mainly high plains, with an average elevation above 1000 m. According to the Third National Land Survey (https://www.nmg.gov.cn/), the main land use types are grassland, forest land, and cropland, with area proportions of 46.00%, 20.00%, and 9.70%, respectively. Land use is characterized by a banded distribution along the Da Hinggan Ling Mountains-Yinshan Mountain range, with a mix of agriculture, livestock, and forestry. Vegetation types are forest, forest-steppe, meadow steppe, typical steppe, desert steppe, and desert from east to west.

2.2 Data collection

Data used in this study were divided into two datasets: one for describing the active fire points and burned area, and the other for comprising the explanatory variables to estimate the probability of fire occurrence (Table 1).

Table 1 Detailed descriptions of data

Type of data	Parameter	Dataset name	Data format	Resolution	Data access
Active fire	Ignition point	MOD14A1/MYD14A1	Raster	1 km	https://www.earthdata.nasa.gov/
	Burned area	MCD64A1	Raster	500 m	
Explanatory variable	Climate	CHN_GMO_MON	Shapefile point	-	https://data.cma.cn/
	Topography	SRTM	Raster	1 km	https://www.resdc.cn/
	Landscape	Land cover	Raster	30 m	https://zenodo.org/
	Anthropogenic	Population	Raster	1 km	https://www.resdc.cn/
		Gross domestic product	Raster	1 km	https://www.resdc.cn/
		Road	Shapefile line	-	http://www.openstreetmap.ch/
		Settlement	Shapefile point	-	
	Vegetation	NDVI	Raster	250 m	https://www.resdc.cn/

Note: CHN_GMO_MON, SRTM, and NDVI are China ground meteorological observation historical dataset (monthly data), Shuttle Radar Topography Mission, and normalized difference vegetation index, respectively. "-" means no resolution.

2.2.1 Burned area and ignition point datasets

Burned area and ignition point from 2000 to 2022 were extracted from MCD64A1, MOD14A1 and MYD14A1 products, which are available on the EARTHDATA website (https://search.earthdata.nasa.gov/). The MCD64A1 dataset has a monthly resolution, a level-3 gridded 500 m product containing the burned area, quality assurance (QA), and tile-level metadata. The pixel values of 1–366 represent the ordinal day of the burning (Giglio et al., 2022). In this study, based on the information provided by the QA layer, we extracted the corresponding burned area when the pixel value of the QA was equal to 3.

The ignition point was obtained from MOD14A1 and MYD14A1 product. For convenience, every 8 d of data were packaged into a single file. The MOD14A1 and MYD14A1 fire mask pixels were divided into 10 levels (Giglio et al., 2021). In previous study, the locations of the ignition point were directly identified when the pixel values of the fire mask layer were equal to 8 and 9 (nominal and high confidence). This result could potentially lead to overestimation of the fire count (He et al., 2023). Therefore, in this study, the following preprocessing steps were carried out on the MOD14A1 and MYD14A1 datasets: (1) the points with a confidence level ≥80 were chosen as true ignition point; (2) we conducted further masking of the fire mask layer based on the information provided by the QA layer (the QA values were equal to 2 and 6); (3) the ignition point was considered in the MOD14A1 dataset if the active fires were detected in the same location in both MOD14A1 and MYD14A1 products; and (4) the ignition point with a time interval ≤1 d and a distance ≤1 km was regarded as part of the same fire event, and the information for earliest detected ignition point was retained.

2.2.2 Explanatory variable datasets

To estimate the active fire occurrence probability, we compiled explanatory variable datasets, including climate, topographic, landscape, anthropogenic, and vegetation data (Table 2). All of the variables were converted to a spatial resolution of 1 km.

The maximum wind speed, maximum air temperature, and relatively humidity, including data from 112 meteorological stations from 2000 to 2022 were collected first at the monthly scale from the National Meteorological Information Center. Then, climate data of spring (March, April, and May), summer (June, July, and August), autumn (September, October, and November), and winter (December, January, and February) seasons were integrated using the mean values of climate parameters. Finally, the fire danger index (FDI) was introduced to reflect the spread of fire and the fuel moisture content (Elia et al., 2020). The formula for calculating FDI is as follows:

$$\mathrm{FDI} = \frac{\max(U)}{\mathrm{FMI}}, \tag{1}$$

where max(U) is the maximum wind speed (km/h); and FMI is the fuel moisture index, which was developed by Sharples et al. (2009). The FMI is defined as follows:

$$\mathrm{FMI} = 10 - 0.25(T - H), \tag{2}$$

where T and H are the maximum air temperature (°C) and relatively humidity (%), respectively.

Table 2 List of explanatory variables

Type	Input parameter	Output parameter	Abbreviation	Variable type
Climate	Maximum wind speed Maximum air temperature Relatively humidity	Fire danger index	FDI	Continuous
Topography	Slope	Slope map	Slo	Continuous
	Elevation	Elevation map	Ele	Continuous
	Aspect	Aspect map	Asp	Categorical
Landscape	Land cover	Land cover map	LC	Categorical
Anthropogenic	Population	Population density	Pop	Continuous
	Gross domestic product	GDP density	GDP	Continuous
	Road	Distance to roads	D-road	Continuous
	Settlement	Distance to settlements	D-set	Continuous
Vegetation	NDVI	NDVI	NDVI	Continuous

Note: The abbreviations are the same as in the following tables.

Topographic factors have been confirmed to have important influences on fire occurrence (Jia et al., 2019). Topographic variables, including slope, aspect, and elevation, were extracted from the Shuttle Radar Topography Mission (SRTM) data. Slope and elevation factors were set as continuous variables, and aspect was set as a categorical variable (Table 3).

Table 3 Specific information about the aspect classification

Aspect	Direction	Classification
Flat	–1.0°	0
Shady slope	North (0.0°–22.5°), northeast (22.5°–67.5°)	1
Semi-shady slope	East (67.5°–112.5°), northwest (292.5°–337.5°)	2
Sunny slope	South (157.5°–202.5°), southwest (202.5°–247.5°)	3
Semi-sunny slope	Southeast (202.5°–247.5°), west (247.5°–292.5°)	4

Annual China land cover (LC) datasets from 2000 to 2022 with a 30-m spatial resolution were used to describe the characteristics of surface landscape (Yang and Huang, 2021). Considering the real LC scenarios in the study area, we classified the landscapes into six types: cropland, forest land, grassland, water body, barren land, and impervious land. Subsequently, LC datasets were upscaled to a 1-km resolution utilizing resampling method.

Seasonal normalized difference vegetation index (NDVI) data from 2000 to 2022 were obtained from the Resource and Environment Data Center (REDC), Chinese Academy of Sciences. High NDVI values indicate dense and healthy vegetation, which can provide abundant fuel for fires. The dense vegetation can support intense and rapidly spreading fires once ignited, especially in areas prone to dry and windy conditions.

Some fires are strongly associated with human activities. Human activities mainly occurred on roads and in urban and rural settlements. Human-related variables, including gross domestic product (GDP), population density (Pop), and distances to roads and settlements, were collected to explain the contribution of human activities to the occurrence of fires. The Pop and GDP variables were derived from the REDC data for 2000, 2005, 2010, 2015, and 2020 with 1-km

resolution. Data for the roads and urban and rural settlements were acquired from the Open Street Map website (http://www.openstreetmap.ch/). The distances of each raster center point from the nearest roads and settlements were extracted using the near analysis tool in the ArcGIS v.3.2 software.

2.2.3 Data standardization

We performed the data standardization based on a specified fuzzification algorithm. Data standardization can accelerate the convergence speed of the fire estimating model and improve the model stability and generalization ability. Explanatory variables (expect for the categorical variables and NDVI factor) were standardized to a 0–1 range.

2.3 Analysis of spatiotemporal variation of active fires

We analyzed the temporal characteristics of ignition point and burned area at the monthly, seasonal, and annual scales. The Manner-Kendall (M-K) test was used to reveal the change trend of active fires. Kernel density, standard deviational ellipse (SDE), and barycenter migration methods were used to clarify the spatial clustering and diffusion characteristics of active fires.

2.4 Estimating probability of active fire occurrence

Before establishing the prediction model, we generated non-fire points datasets using the creating random point tool in ArcGIS software, and set the value of 1 as ignition point and the value of 0 as non-fire point. Distance between each pair of random points was greater than 2 km in order to ensure that the non-fire points did not overlap and did not fall within the burned area. We set the ratio of ignition point to non-fire point as 1:3 according to the total number of seasonal ignition point. Next, point dataset was divided into training (70.00% of data) and testing (30.00% of data) sets using randomly selecting approach.

Taking into account the seasonal characteristics of the fire occurrence, we chose four models, namely, logistic regression (LR), random forest (RF), support vector machine (SVM), and convolutional neural network (CNN) models, to estimate the probability of active fire occurrence at the seasonal scale in Python v.3.12 software.

LR model has been widely used to predict the probability and analyze the driving factors of fire occurrence using a logit function. RF model operates by constructing a multitude of decision trees during training and outputting the mode of classes or prediction of individual trees, and it has been proven to have high reliability in terms of variable importance screening. SVM model is effective in high dimensional spaces and supports different kernel functions for nonlinear classification.

CNN model is a class of deep learning algorithm that was specifically designed to process structured grid data such as images. We used TensorFlow v.2.15 software to train and implement CNN model. Structure of CNN model consisted of three convolutional layers, three maximum pooling layers, and three fully connected layers. The numbers of kernels in convolutional layers 1–3 were 64, 128, and 256, respectively. The size of kernel was 3×3 for all of the layers, and the step size was set to 1. Each convolutional layer was followed by a batch normalization layer and a maximum pooling layer. This structural design helps to extract features and reduce overfitting. The size of kernel was 2×2 in the maximum pooling layers, and the step size was 2. Numbers of neurons in fully connected layers 1–3 were set to 128, 64, and 32, respectively.

2.5 Evaluation of variable importance and model performance

Shapely additive explanations (SHAP) method was utilized to evaluate the importance of variables in the fire occurrence models. Accuracy and area under receiver operating characteristic curve (AUC) were introduced as metrics to assess the performances of fire prediction models. Accuracy represents the ratio of correct predictions to overall number of samples. Range of AUC values is between 0.500 and 1.000. An AUC value closer to 1.000 indicates a better model performance, while an AUC of 0.500 indicates no discrimination ability. An AUC value greater than 0.700 indicates that the explanatory variables predict the dependent variable well.

3 Results

3.1 Spatiotemporal dynamics of active fires

3.1.1 Temporal characteristics of active fires

Monitoring results in the MODIS thermal anomalies/fire products datasets revealed that a total of 100,343 active fires occurred in Inner Mongolia from 2000 to 2022, with a cumulative burned area of 6.59×10^4 km^2. Overall, number of ignition point exhibited a significant increasing trend, while burned area exhibited a nonsignificant decreasing trend (Fig. 1a). The M-K test revealed that ignition point exhibited a nonsignificant decreasing trend from 2000 to 2002, followed by a nonsignificant increasing trend from 2003 to 2009. A break point occurred in 2008, and a significant increasing trend was observed after 2010. Burned area exhibited a nonsignificant increasing trend after 2003, 2008, and 2014, and it exhibited a nonsignificant decreasing trend in the other years (Fig. 1b).

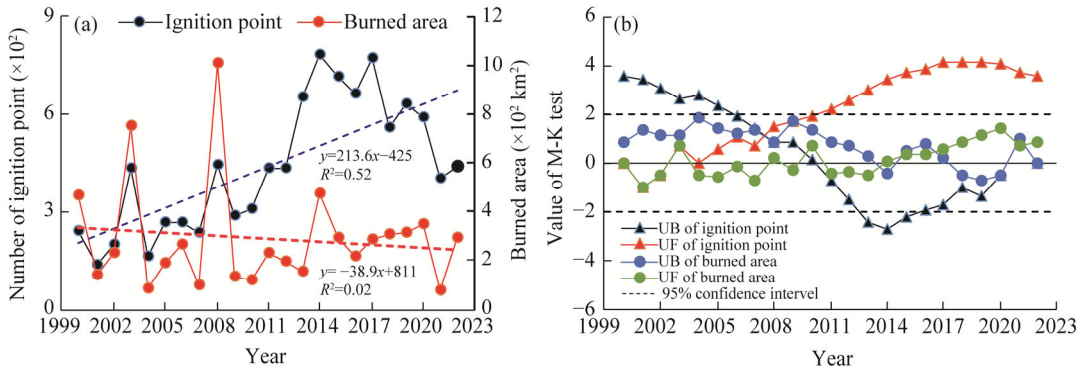

Fig. 1 Annual dynamics (a) and Manner-Kendall (M-K) test results (b) of ignition point and burned area. UF and UB stand for the forward sequence statistic and backward sequence statistic, respectively.

Fire occurrences were the highest in spring, followed by those in autumn and summer, and they were the lowest in winter (Table 4). Change in burned area was consistent with fire occurrences. Approximately 81.36% of fire occurrences contributed to 86.97% of burned area in spring and autumn. In spring, number of ignition point and burned area decreased successively from March to May. In autumn, number of ignition point was the highest in October, and burned area was the largest in September. In summer, both ignition point and burned area decreased in the sequence

Table 4 Contribution rates of ignition point and burned area at the seasonal and monthly scales

Season	Seasonal contribution rate (%)		Month	Monthly contribution rate (%)	
	Ignition point	Burned area		Ignition point	Burned area
			Mar	49.08	57.94
Spring	49.65	67.88	Apr	37.53	27.91
			May	13.39	14.14
			Jun	29.02	22.76
Summer	12.23	9.77	Jul	27.97	19.55
			Aug	43.01	57.68
			Sep	31.65	60.91
Autumn	31.61	18.09	Oct	49.51	22.79
			Nov	18.84	16.29
			Jan	14.23	4.89
Winter	6.51	4.26	Feb	72.31	94.23
			Dec	13.46	0.88

of August, June, and July. In winter, 72.31% of ignition point in February contributed to 94.23% of burned area.

Table 5 illustrates the changes in ignition point and burned area in different ecosystems. Ignition point was primarily concentrated in grassland and cropland. Proportions of fire occurrences in these ecosystems were 48.55% and 40.09%, respectively, and proportions of burned area were 56.35% and 37.25%, respectively. Fire occurrences in forest land and urban land accounted for 11.36%, and proportion of burned area was about 6.40%.

Table 5 Proportions of ignition point and burned area in different land use types

Index	Forest land	Grassland	Cropland	Urban land
Ignition point (%)	1.76	48.55	40.09	9.60
Burned area (%)	5.31	56.35	37.25	1.09

3.1.2 Spatial distribution characteristics of active fires

From the result of kernel density of ignition point, we classified the spatial distribution of active fires into four fire belts in Inner Mongolia: (I) Hetao-Tumochuan Plain fire belt; (II) Xiliao River Plain fire belt; (II) Songnen Plain fire belt; and (IV) Hailar River Eroded Plain fire belt (Fig. 2a).

We computed the SDE and plotted the centroid migration trajectory of active fires to reveal the spatial diffusion characteristics of active fires in Inner Mongolia during different stages (Fig. 2b). Azimuth of the SDE changed by approximately 5.2°. Increase in standard deviation along major axis was significantly higher than that of minor axis. These results demonstrate that the direction in which the fires spread, along the direction from north-northeast to south-southwest, gradually strengthened during spatial diffusion process. Average centroid shifted 151.9 km toward southwest when active fires transitioned from a nonsignificant decreasing phase (2000–2002) to a nonsignificant increasing phase (2003–2009). Average centroid subsequently shifted 304.5 km to southwest after active fire occurrences entered a significant increasing phase (2010–2022; Fig. 2b).

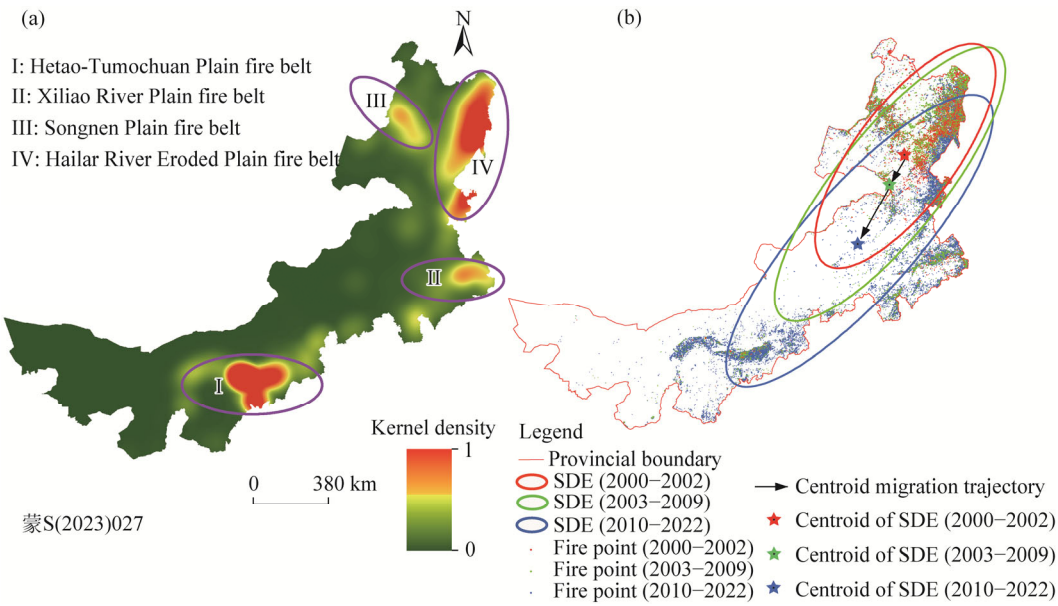

Fig. 2 Spatial distribution of active fires from 2000 to 2022. (a), kernel density; (b), standard deviational ellipse (SDE) and centroid migration trajectory. The figures are based on the standard map (蒙 S(2023)027) of Department of Natural Resources of Inner Mongolia Autonomous Region (https://zrzy.nmg.gov.cn/bsfw/bzdt/nmgzzqbzdt/), and the boundary of the standard map has not been modified.

3.2 Estimating the probability of active fire occurrence

3.2.1 Performance of model fitting and importance of variables

We calculated the accuracy and AUC values for LR, RF, SVM, and CNN models at the seasonal scale from 2000 to 2022 and recorded their minimum, maximum, and average values to test the predictive capabilities of these four models in determining the probability of active fire occurrence (Table 6). In general, the minimum accuracy and AUC values were 83.30% and 0.864, respectively, indicating that all four models had good predictive capabilities for fire occurrences at the seasonal scale. For all of the models, accuracy of fire occurrence estimation was significantly higher in spring and autumn than in summer and winter. We found that RF model had the highest predictive accuracy, followed by CNN model, and LR and SVM models had lower accuracies.

Table 6 Performance metrics of the four fire prediction models at the seasonal scale

Model	Data type	Spring		Summer		Autumn		Winter	
		Accuracy (%)	AUC	Accuracy (%)	AUC	Accuracy (%)	AUC	Accuracy (%)	AUC
LR	Minimum	86.00	0.912	83.90	0.906	84.90	0.895	83.30	0.922
	Maximum	92.50	0.968	92.30	0.969	91.60	0.962	98.60	0.994
	Average	89.80	0.944	89.00	0.940	89.30	0.940	91.60	0.960
RF	Minimum	91.70	0.964	90.50	0.943	93.60	0.971	83.30	0.948
	Maximum	96.80	0.991	95.70	0.990	96.10	0.991	99.30	0.981
	Average	94.30	0.980	94.00	0.976	95.00	0.984	94.80	0.983
SVM	Minimum	85.40	0.906	84.70	0.896	84.30	0.864	83.30	0.883
	Maximum	92.70	0.969	93.60	0.973	91.50	0.962	96.40	0.997
	Average	89.50	0.943	89.30	0.939	89.30	0.936	91.70	0.959
CNN	Minimum	90.30	0.950	85.70	0.918	89.30	0.938	83.30	0.870
	Maximum	94.40	0.980	93.60	0.967	94.30	0.981	98.60	0.993
	Average	92.20	0.966	90.50	0.954	92.20	0.966	92.80	0.968

Note: LR, logistic regression; RF, random forest; SVM, support vector machine; CNN, convolutional neural network; AUC, accuracy and area under receiver operating characteristic curve.

To analyze the importance of explanatory variables in fire prediction models, we computed the shapely values using SHAP method. Next, shapely values were ranked in descending order, and frequency of each variable's appearance was recorded. Finally, we identified which factor contributed the most to the model's predictions based on frequency. Table 7 showed that although the four models differed significantly in terms of their principles for fire prediction, they exhibited similar characteristics in identifying the importance of explanatory variables. Natural factors (e.g., elevation and FDI) had higher importance, followed by variables related to human activities (e.g., population density, and distances to roads and settlements), and aspect variable had the lowest importance in spring and autumn. Variables related to human activities had higher importance, followed by natural factors. Importance of slope and aspect was relatively low in summer and winter.

3.2.2 Probability of active fire occurrence

We mapped probability of active fire occurrence in Inner Mongolia over the past 20 a based on four predictive models (Figs. S1–S6). In this study, we utilized RF model, which achieved the highest estimation accuracy, to investigate probability of active fire occurrence (Figs. 3 and 4). Probability ranged from 0.0 to 1.0. Fire risk level was classified into five levels using an equal interval method: low risk (0.0–0.2), moderately low risk (0.2–0.4), moderately high risk (0.4–0.6), high risk (0.6–0.8), and extremely high risk (0.8–1.0).

High and extremely high fire risk areas were mainly distributed in Hetao-Tumochuan Plain,

Table 7 Ranking of variables' importance in LR, RF, SVM, and CNN models at the seasonal scale

Rank	LR				RF				SVM				CNN			
	Spring	Summer	Autumn	Winter	Spring	Summer	Autumn	Winter	Spring	Summer	Autumn	Winter	Spring	Summer	Autumn	Winter
1	Ele	D-road	FDI	GDP	Ele	D-road	FDI	Pop	Ele	GDP	FDI	GDP	Ele	D-road	FDI	GDP
2	FDI	FDI	Pop	D-set	FDI	Pop	Ele	GDP	FDI	FDI	Pop	Pop	FDI	GDP	Ele	D-road, Pop
3	LC-5	GDP	Ele, LC-5	GDP	Pop	GDP	GDP, Pop	D-road	Pop	GDP	Ele	D-road	FDI	FDI	NDVI	LC-3
4	D-set	GDP	NDVI	LC-3	LC-1	Pop	LC-1	D-set	LC-2, LC-3	LC-3	LC-1	FDI, LC-3	LC-3	Pop	LC-3	NDVI
5	NDVI	Ele	Slo	FDI	GDP	FDI	GDP	D-road	D-set	D-set	LC-3	LC-2, D-set	LC-3	NDVI	LC-3	D-road
6	D-road	LC-5	LC-3	NDVI	D-road	LC-6	GDP	Ele	LC-1	NDVI	LC-3	LC-3	D-road	LC-3	Slo, D-road	NDVI
7	LC-3	LC-6	LC-3	LC-3	LC-3	LC-6	D-road, D-set	NDVI	LC-5	LC-6	LC-3	LC-1	D-set	Asp-1	D-set	FDI
8	LC-1	LC-6	LC-2	LC-1, LC-2	D-set	Ele	Slo, LC-3	NDVI	NDVI	Ele	LC-2, Slo	LC-2	LC-5	Slo	Slo	LC-5
9	GDP, Pop	LC-3	Slo	Asp-1	D-set	LC-1	LC-3	Slo	Slo	LC-5	NDVI	FDI	Slo	LC-5	Slo	LC-1, Slo
10	Slo	LC-1, Slo	D-road	Asp-1	Slo	Slo	Slo	NDVI	Asp-1, Asp-4	Asp-2	LC-6	Ele, Asp-1	LC-1	Slo	D-set	LC-5
11	D-road	Asp-4	LC-6	LC-5	LC-5	LC-3	LC-6	LC-6	Asp-3	Asp-4	D-road, Asp-3	LC-6	Slo	Asp-1	LC-2	LC-5
12	LC-2	Asp-2	Asp-5	LC-5	LC-6	LC-5	LC-2	Asp-1	Asp-1	Asp-1	LC-6	Asp-3	Asp-1	Asp-2	Asp-1	Asp-2
13	Asp-3, Asp-4	LC-1, Slo	Asp-2	Asp-2, Asp-3	LC-2	LC-5	LC-2	LC-5	Asp-2	LC-1	Asp-4	Asp-4	Asp-2	LC-5	Asp-3	Asp-2
14	Asp-1	Asp-3	Asp-3	Asp-4	Asp-3	Asp-2	Asp-4	Asp-1	Asp-4	Asp-4	Asp-2	Asp-2	LC-2	LC-2	Asp-4	LC-6
15	Asp-2	Asp-1	Asp-2	LC-6	Asp-1	Asp-3	Asp-1	Asp-2	Asp-3	Asp-2	Asp-4	Asp-2	Asp-3	Asp-4	LC-5	LC-2, Asp-4
16	Asp-2	Asp-1	Asp-2	Asp-4	Asp-1	Asp-4	Asp-2	Asp-4	Asp-2	Asp-2	Asp-1	Asp-2	LC-2	LC-1	Asp-2	Asp-1
17	LC-4, Asp-0	LC-4	LC-4	Asp-2	Asp-2	Asp-1	Asp-3	Asp-4	LC-4	LC-4	LC-4	Asp-4	LC-6	LC-1	LC-6	LC-6
18	LC-4	Asp-0	Asp-0	Asp-0	LC-4	Asp-0	Asp-0	Asp-0	Asp-0	Asp-0	LC-4	Asp-0	Asp-0	Asp-0	LC-4	Asp-0
19	Asp-0	LC-4	LC-4	LC-4	Asp-0	LC-4	LC-4	LC-4	Asp-0	LC-4	Asp-0	LC-4	LC-4	LC-4	Asp-0	LC-4

Note: LC-1–LC-6 are cropland, forest land, grassland, water body, barren land, and impervious land, respectively; Asp-0–Asp-4 are flat, shady slope, semi-shady slope, sunny slope, and semi-sunny slope, respectively.

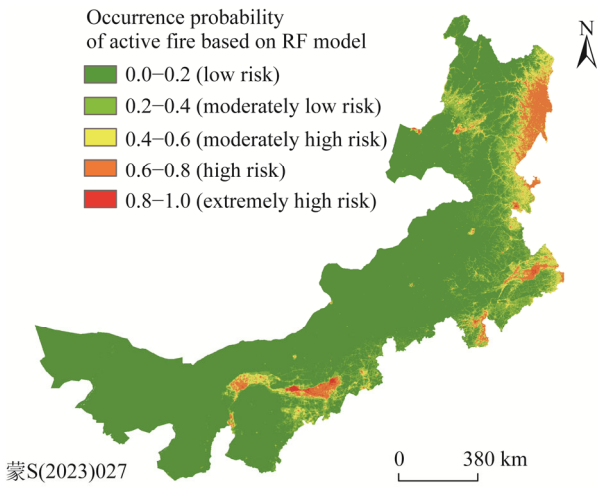

Fig. 3 Spatial distribution of fire risk level based on random forest (RF) from 2000 to 2022

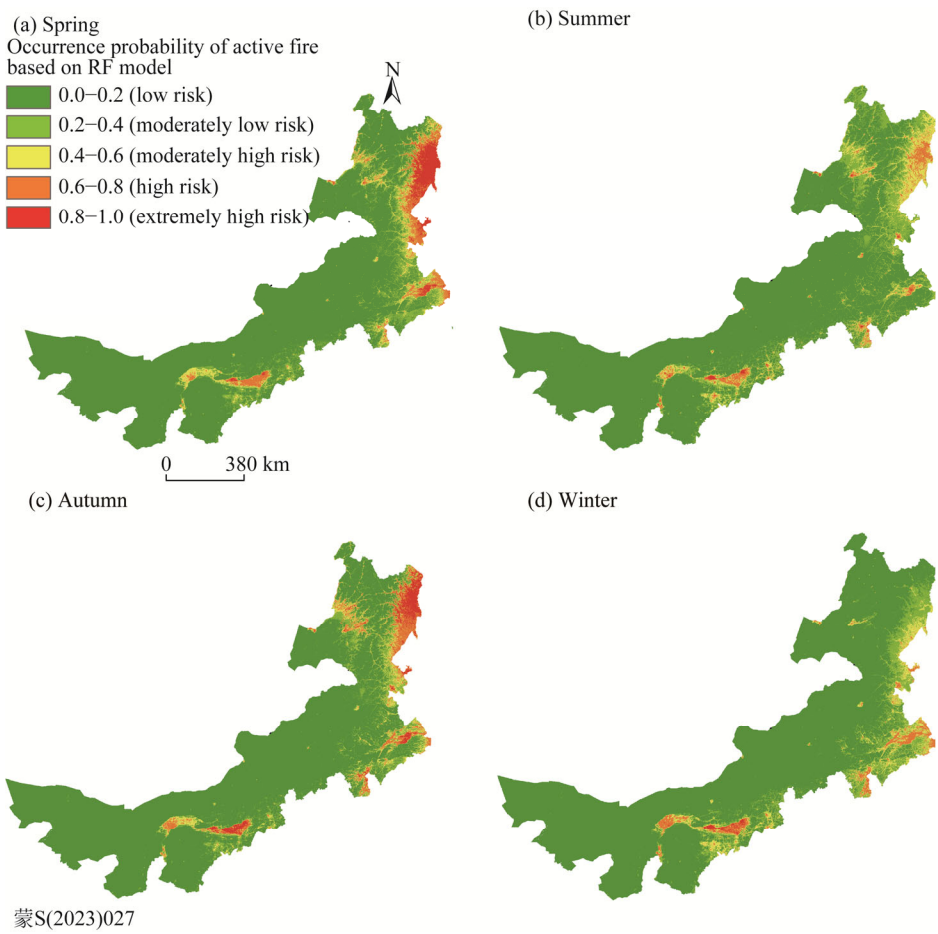

Fig. 4 Spatial distribution of fire risk level based on RF model at the seasonal scale. (a), spring; (b), summer; (c), autumn; (d), winter.

north of the Yellow River, Xiliao River Plain in Tongliao City, Laoha River in Chifeng City, eastern Hulun Buir City, the Hinggan League, and the plains in western foothills of the Da Hinggan Ling Mountains (Fig. 3). Area with a moderately high risk accounted for approximately 10.10% of the study area. Spatial distribution of fire occurrence risk at the seasonal scale was

similar to that at the annual scale (Fig. 4). Probability of fire occurrence in Inner Mongolia was the highest in spring, followed by that in autumn, and it gradually decreased in summer and winter. Proportions of the areas with moderately high risk were 11.80%, 11.20%, 8.50%, and 7.50% in spring, autumn, summer, and winter, respectively.

4 Discussion

4.1 Spatotemporal patterns of active fires

Inner Mongolia has experienced severe fire disturbances due to human activities and climate change (Sun et al., 2021; Chang et al., 2023). Thus, we utilized the MODIS active fire products to reveal the fire regime in Inner Mongolia from 2000 to 2022. Number of active fires has shown a declining trend at global scale from the perspective of remote sensing observations since 2000 (Earl and Simmonds, 2018). But the opposite trend occurred in China (Wei et al., 2020). Similarly, we also found that ignition point exhibited a significant increasing trend in Inner Mongolia. Ignition point mainly occurred in grassland and cropland ecosystems, and four active fire belts were detected surrounding the agricultural production areas. Smoking and agricltural fires, such as slash-and-burn land clearing and straw burning, in the grassland and cropland were the primary causes of fires in spring and autumn based on historical statistics on fires (Zhang et al., 2024c). It should be noted that a significant decline in cropland and grassland fire occurrences has been observed since 2015. This notable reduction was primarily due to a series of measures implemented by the government of Inner Mongolia in response to the Atmospheric Pollution Prevention and Control Law of China, including intensified supervision and law enforcement, as well as efforts to raise public awareness of straw burning bans and related regulations.

Our findings indicated that active fire centroid shifted by 456.4 km from northeast to southwest. Liu et al. (2023a) argued that significant decrease in vegetation fire occurrences in Hulun Buir City, located in northeastern part of the study area, between 2003 and 2019—along with the lack of a notable increase in other leagues—was the main reason for southwestward shift of the fire centroid. In addition, the direction of fire spread was north-northeast to south-southwest, and this trend gradually strengthened during the study period. This result may imply an increase in the regularity and predictability of fire occurrence and spread in Inner Mongolia, and it may also reflect the long-term impacts of certain climate changes and human activities (Zhang et al., 2024a).

Although ignition point exhibited a significant increasing trend, burned area exhibited a decreasing trend in Inner Mongolia. Previous studies have shown that global burned area decreased by 24.30% (±8.80%) from 1998 to 2015 (Andela et al., 2017). The areas that experienced a significant decrease in burned area were mainly distributed in tropical and temperate zones (Senande-Rivera et al., 2022). Inner Mongolia is located in mid-temperate climate zone, and human activities, such as strengthened fire source control and improved fire monitoring and early warning capabilities, have been the dominant factor contributing to the declining trend in burned area (Hayes, 2020; Qin et al., 2020).

4.2 Fire occurrence probability analysis

Our results revealed that RF model had the highest accuracy, followed by CNN, and LR and SVM models had lower accuracies. Previous studies have demonstrated that RF model performed well in predicting fire occurrence probability compared with other approaches (Li et al., 2023; Gao et al., 2024). Advantages of RF model lie in its flexibility and robustness, particularly in handling nonlinear, noisy, and complex data (Fawagreh et al., 2014). In contrast, SVM, CNN, and LR models are prone to overfitting when dealing with complex data and have lower noise resistance (Pang et al., 2022). Another important reason may be that a relatively sufficient number of training samples were used and appropriate multidimensional variables were screened out in fire occurrence probability modeling. Although CNN model also achieved a good accuracy in this study, its computational efficiency was lower than that of the other prediction models. In future

studies, an important task will be to continually optimize the configuration of convolutional layers, pooling layers, fully connected layers, and parameters such as batch size to make the CNN model a robust tool for fire prediction.

Moreover, four prediction models exhibited similar characteristics during the process of selecting feature variables. Natural factors (e.g., FDI and elevation) had a higher importance in spring and autumn, while variables related to human activities (e.g., population density, GDP, and distances to roads and settlements) were more significant in summer and winter. FDI, which combines the maximum wind speed and fuel moisture index, provides a quantitative measure of potential fire risk in a specific area (Elia et al., 2020). Areas with elevated FDI values are generally associated with higher fire risk. Climate in Inner Mongolia is often dry and windy in spring and autumn. With the intensification of global warming, frequency of extreme drought and high-temperature events has increased significantly, resulting in the production of a large amount of flammable material via vegetation wilting (Chen et al., 2022). This phenomenon greatly enhances the probability of fire occurrence, making FDI an important feature variable. At the same time, ditribution of fires showed a significant corrrelation with topographic factors and exhibited a distinct gradient pattern (Guan et al., 2025). For example, Jia et al. (2019) found that most fire occurrences were primarily concentrated at elevations ranging from 80 and 700 m in Inner Mongolia, and this topographic feature could significantly accelerate the spread of fires, particularly under strong wind conditions. Rainfall is relatively abundant in summer, and human activities in tourist areas and along transportation routes increase the probability of fire occurrences. Furthermore, the use of heating equipment and agricultural activities such as slash-and-burn could also increase the risk of fire in winter, particularly in rural areas with high population density.

4.3 Limitations and prospects

Although probability and spatiotemporal dynamics of active fire occurrence in Inner Mongolia were analyzed using remote sensing data, several limitations remained in this study. First, owing to the absence of ground-based fire observation data, accuracy of MODIS burned area products was not assessed by observation data, and the quantitative interpretation of fire-driving mechanisms was not provided. Meanwhile, MODIS active fire products have a relatively coarse spatial resolution, making it difficult to detect small-scale fires. Accordingly, it is necessary to develop long-term and high spatial resolution burned area products using time-series Landsat and Sentinal imagery for precise and effective fire monitoring. Second, some explanatory variables were simplified during the process of estimating fire occurrence probability, which may have affected the accuracy of fire risk mapping. For instance, NDVI variable was used as a proxy indicator to measure spatial distribution of fuel load. During analyzing the influence of human activities on fire occurrence, we incorporated static variables including population density and GDP at 5-a intervals, which might affect the accuracy. Future studies could integrate real-time and higher frequency variables to improve the accuracy of fire prediction.

5 Conclusions

We systematically analyzed the spatiotemporal dynamics of active fire in Inner Mongolia based on MODIS fire products from 2000 to 2022 and estimated the probability of fire occurrence at the seasonal scale using LR, RF, SVM and CNN models. The results indicated that while number of fire incidents in Inner Mongolia exhibited a significant upward trend, burned area showed a decreasing trend. Meanwhile, four active fire belts were identified surrounding the agricultural production areas. Fire management efforts should be enhanced in Inner Mongolia, particularly for fires occurring in cropland and grassland ecosystems in spring and autumn. Moreover, average fire centroid has shifted southwestward, reflecting the combined effects of climate change and human activity. Finally, RF and CNN models demonstrated superior predictive performance for active fire occurrences compared with LR and SVM models. This result provides a research

foundation for future efforts to estimate fire occurrence probability in Inner Mongolia under different climate change scenarios. In summary, these findings hold important practical and policy implications for optimizing fire prevention resource allocation, refining risk management strategies, and enhancing regional ecological security in Inner Mongolia.

Conflict of interest

The authors declare that they have no known competing financial interests or personal relationships that could have appeared to influence the work reported in this paper.

Acknowledgements

This research was funded by the First-Class Discipline Research Special Project of Inner Mongolia (YLXKZX-NSD-040), the Natural Science Foundation of Inner Mongolia (2022LHQN04003, 2023QN04009), the Fundamental Research Funds for the Inner Mongolia University of Finance and Economics (NCXKY25019, NCYWZ22003), and the National Social Science Fund of China (22BZS134).

Author contributions

Writing - original draft preparation: JIA Xu, WEI Baocheng; Writing - review and editing: JIA Xu, WEI Baocheng, ZHANG Zhijie, WANG Jing; Resources and Software: ZHANG Zhijie, CHEN Lulu, LIU Mengna, ZHAO Yiming; Supervision: WEI Baocheng; Methodology: CHEN Lulu, LIU Mengna, ZHAO Yiming. All authors approved the manuscript.

References

Aldersley A, Murray S J, Cornell S E. 2011. Global and regional analysis of climate and human drivers of wildfire. Science of the Total Environment, 409(18): 3472–3481.

Andela N, Morton D, Giglio L, et al. 2017. A human-driven decline in global burned area. Science, 356(6345): 1356–1362.

Belarbi F, Hassini A, Benamara N K. 2024. A novel approach based on convolutional neural networks ensemble for fire detection. Signal, Image and Video Processing, 18: 8805–8818.

Chang C, Chang Y, Xiong Z P, et al. 2023. Predicting grassland fire-occurrence probability in Inner Mongolia Autonomous Region, China. Remote Sensing, 15(12): 2999, doi: 10.3390/rs15122999.

Chao L M, Bao Y L, Zhang J Q, et al. 2023. Quantitative assessment of fire occurrence dead fuel index threshold and spatio-temporal variation in different grassland types of China-Mongolia border area. Journal of Geographical Sciences, 33(8): 1631–1659.

Chao Y, Luo C F, Shu L F, et al. 2020. A review on wildfire studies in the context of global change. Acta Ecologica Sinica, 40(2): 385–401. (in Chinese)

Chen K, Ge G, Bao G, et al. 2022. Impact of extreme climate on the NDVI of different steppe areas in Inner Mongolia, China. Remote Sensing, 14(7): 1530, doi: 10.3390/rs14071530.

Chen X T, Kang S C, Hu Y L, et al. 2023. Temporal and spatial analysis of vegetation fire activity in the circum-Arctic during 2001–2020. Research in Cold and Arid Regions, 15(1): 48–56.

Duan Q, Liu R G, Chen J L, et al. 2024. Burned area detection from a single satellite image using an adaptive thresholds algorithm. International Journal of Digital Earth, 17(1): 2376275, doi: 10.1080/17538947.2024.2376275.

Earl N, Simmonds I. 2018. Spatial and temporal variability and trends in 2001–2016 global fire activity. Journal of Geophysical Research: Atmospheres, 123(5): 2524–2536.

Elia M, D'Este M, Ascoli D, et al. 2020. Estimating the probability of wildfire occurrence in Mediterranean landscapes using Artificial Neural Networks. Environmental Impact Assessment Review, 85: 106474, doi: 10.1016/j.eiar.2020.106474.

Ellis T M, Bowman D M J S, Jain P, et al. 2021. Global increase in wildfire risk due to climate-driven declines in fuel moisture. Global Change Biology, 28(4): 1544–1559.

Fawagreh K, Gaber M M, Elyan E. 2014. Random forests: from early developments to recent advancements. Systems Science & Control Engineering, 2(1): 602–609.

Gao B, Shan Y L, Liu X Y, et al. 2024. Prediction and driving factors of forest fire occurrence in Jilin Province, China. Journal of Forestry Research, 35(1): 21, doi: 10.1007/s11676-023-01663-w.

Giglio L, Humber M, Hall J V, et al. 2022. Collection 6.1 MODIS burned area product user's guide version 1.1. In: NASA

Technical Report. University of Maryland. Maryland, USA.

Giglio L, Schroeder W, Hall J V, et al. 2021. MODIS collection 6 and collection 6.1 active fire product user's guide version 1.0. In: NASA Technical Report. University of Maryland. Maryland, USA.

Guan R H, Jiao K W, Chang Y, et al. 2025. Spatiotemporal dynamics of wildland urban interface distribution patterns and high fire occurrence areas in Heilongjiang Province. Acta Ecologica Sinica, 45(13): 1–11. (in Chinese)

Haas O, Prentice I C, Harrison S P. 2022. Global environmental controls on wildfire burnt area, size, and intensity. Environmental Research Letters, 17(6): 065004, doi: 10.1088/1748-9326/ac6a69.

Hayes J P. 2020. Fire suppression and the wildfire paradox in contemporary china: Policies, resilience, and effects in Chinese fire regimes. Human Ecology, 49(1): 19–32.

He R, Lu H, Jin Z Z, et al. 2023. Construction of forest fire prediction model and driving factors analysis based on random forests algorithm in Southwest China. Acta Ecologica Sinica, 43(22): 9356–9370. (in Chinese)

Jain P, Barber Q E, Taylor S W, et al. 2024. Drivers and impacts of the record breaking 2023 wildfire season in Canada. Nature Communications, 15(1): 6764, doi: 10.1038/s41467-024-51154-7.

Jia X, Gao Y, Wei B C, et al. 2019. Risk assessment and regionalization of fire disaster based on analytic hierarchy process and MODIS data: A case study of Inner Mongolia, China. Sustainability, 11(22): 6263–6279.

Jones M W, Kelley D I, Burton C A, et al. 2024. State of wildfires 2023–2024. Earth System Science Data, 16(8): 3601–3685.

Kiely L, Neyestani S E, Binte-Shahid S, et al. 2024. California case study of wildfires and prescribed burns: $PM_{2.5}$ emissions, concentrations, and implications for human health. Environmental Science & Technology, 58(12): 5210–5219.

Li M L, Wu Y D, Liu Y L, et al. 2024. Study on the driving factors of the spatiotemporal pattern in forest lightning fires and 3D fire simulation based on cellular automata. Forests, 15(11): 1857, doi: 10.3390/f15111857.

Li S X, Zhang F Q, Lin H F. 2023. Research on forest fire risk evaluation based on machine learning algorithm. Journal of Nanjing Forestry University, 47(5): 49–56. (in Chinese)

Li Y P, Zhao J J, Guo X Y, et al. 2017. The influence of land use on the grassland fire occurrence in the northeastern Inner Mongolia Autonomous Region, China. Sensors, 17(3): 437, doi: 10.3390/s17030437.

Liu H X, Qian Y L, Kong J J, et al. 2023a. Temporal and spatial variations of vegetation fires in Inner Mongolia from 2003 to 2019 based on FIRMS_MODIS. Forestry Science and Technology Information, 55(1): 1–8. (in Chinese)

Liu L Y, Miao Z L, Wu L X. 2022. Spatial-temporal variability of amazon tropical rainforest fire based on MODIS data. Remote Sensing Technology and Application, 37(3): 721–730. (in Chinese)

Liu W J, Guan H D, Hesp P A, et al. 2023b. Remote sensing delineation of wildfire spatial extents and post-fire recovery along a semi-arid climate gradient. Ecological Informatics, 78: 102304, doi: 10.1016/j.ecoinf.2023.102304.

MacCarthy J, Tyukavina A, Weisse M J, et al. 2024. Extreme wildfires in Canada and their contribution to global loss in tree cover and carbon emissions in 2023. Global Change Biology, 30(6): e17392, doi: 10.1111/gcb.17392.

McNorton J R, Di Giuseppe F. 2024. A global fuel characteristic model and dataset for wildfire prediction. Biogeosciences, 21(1): 279–300.

Milanović S, Marković N, Pamučar D, et al. 2020. Forest fire probability mapping in eastern Serbia: Logistic regression versus random forest method. Forests, 12(1): 5, doi: 10.3390/f12010005.

Monjaras-Vega N A, Briones-Herrera C I, Vega-Nieva D J, et al. 2020. Predicting forest fire kernel density at multiple scales with geographically weighted regression in Mexico. Science of the Total Environment, 718: 137313, doi: 10.1016/j.scitotenv.2020.137313.

Pang Y Q, Li Y D, Feng Z K, et al. 2022. Forest fire occurrence prediction in China based on machine learning methods. Remote Sensing, 14(21): 5546, doi: 10.3390/rs14215546.

Pausas J G, Keeley J E. 2021. Wildfires and global change. Frontiers in Ecology and the Environment, 19(7): 387–395.

Qarallah B, Othman Y A, Al-Ajlouni M, et al. 2022. Assessment of small-extent forest fires in semi-arid environment in Jordan using Sentinel-2 and Landsat sensors data. Forests, 14(1): 41, doi: 10.3390/f14010041.

Qin X L, Li X T, Liu S C, et al. 2020. Forest fire early warning and monitoring techniques using satellite remote sensing in China. Journal of Remote Sensing, 24(5): 511–520. (in Chinese)

Ren X H, Yu R H, Liu X Y, et al. 2022. Spatial changes and driving factors of lake water quality in Inner Mongolia, China. Journal of Arid Land, 15(2): 164–179.

Senande-Rivera M, Insua-Costa D, Miguez-Macho G. 2022. Spatial and temporal expansion of global wildland fire activity in response to climate change. Nature Communications, 13(1): 1208, doi: 10.1038/s41467-022-28835-2.

Sharples J J, McRae R H D, Weber R O, et al. 2009. A simple index for assessing fire danger rating. Environmental Modelling & Software, 24(6): 764–774.

Sun H C, Wang W J, Liu Z H, et al. 2021. The relative importance of driving factors of wildfire occurrence across climatic

gradients in the Inner Mongolia, China. Ecological Indicators, 131: 108249, doi: 10.1016/j.ecolind.2021.108249.

Touge Y, Shi K, Nishino T, et al. 2024. Spatial temporal characteristics of more than 50,000 wildfires in Japan from 1995 to 2020. Fire Safety Journal, 142: 104025, doi: 10.1016/j.firesaf.2023.104025.

Vouzoglanis C K, Reinke K J, Berelov S M, et al. 2024. Are fire intensity and burn severity associated? Advancing our understanding of FRP and NBR metrics from Himawari-8/9 and Sentinel-2. International Journal of Applied Earth Observation and Geoinformation, 127: 103673, doi: 10.1016/j.jag.2024.103673.

Wang W J, Qian C, Zhang Y, et al. 2022. Multi-time scale features of fire weather in two major forests in China during 1961–2020. Climatic and Environmental Research, 27(5): 559–577. (in Chinese)

Wei X K, Wang G J, Chen T X, et al. 2020. A spatiotemporal analysis of active fires over China during 2003–2016. Remote Sensing, 12(11): 1787, doi: 10.3390/rs12111787.

Yang J, Huang X. 2021. The 30 m annual land cover dataset and its dynamics in China from 1990 to 2019. Earth System Science Data, 13(8): 3907–3925.

Zhai J X, Li Y, Zhang B, et al. 2022. Analysis of forest fires and lightning fires in representative fire-prone countries over the world. Journal of Subtropical Resources and Environment, 17(4): 72–79. (in Chinese)

Zhang H, Jia W F, Wang Y N. 2024a. The spatiotemporal dynamics of wildfires in Inner Mongolia based on global fire atlas remote sensing data. Journal of Wildland Fire Science, 42(3): 9–15. (in Chinese)

Zhang H, Li H, Zhao P W. 2024b. Risk of forest fire occurrence in Inner Mongolia and the impact of its drivers. Acta Ecologica Sinica, 44(13): 5669–5683. (in Chinese)

Zhang H, Zhou Z D, Wang Y X. 2024c. Temporal and spatial distribution characteristics of forest fires caused by 3 main fire sources in Daxing'an Mountains, Inner Mongolia. Journal of Southwest Forestry University, 44(3): 166–174. (in Chinese)

Zhang H, Liang Y S, Ren H Y, et al. 2025. Comparing grassland fire drivers and models in Inner Mongolia using field and remote sensing data. Fire, 8(3): 93, doi: 10.3390/fire8030093.

Zhang J Y, Peng D L, Zhan C J, et al. 2024d. Deep learning based forest fire prediction model research in the Daxing'anling Mountains, Inner Mongolia. Forest Research, 37(1): 31–40. (in Chinese)

Zheng X X, Sun N, Luo F. 2024. Spatiotemporal feature of active fire occurrence on the Loess Plateau from 2001 to 2020 based on MODIS. Quaternary Sciences, 44(1): 191–200. (in Chinese)

Appendix

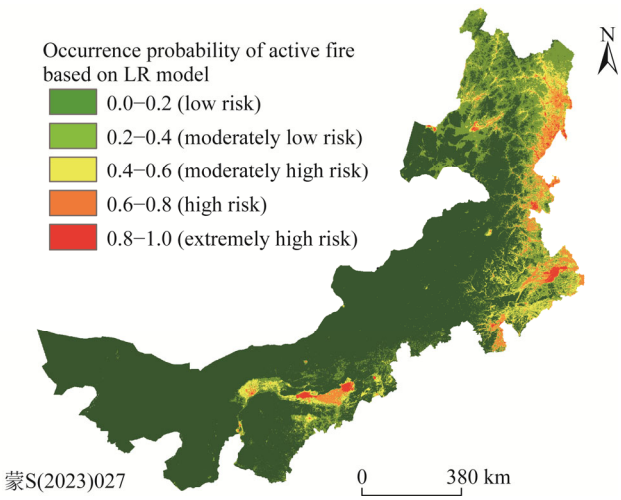

Fig. S1 Spatial distribution of fire risk level based on logistic regression (LR) model from 2000 to 2022

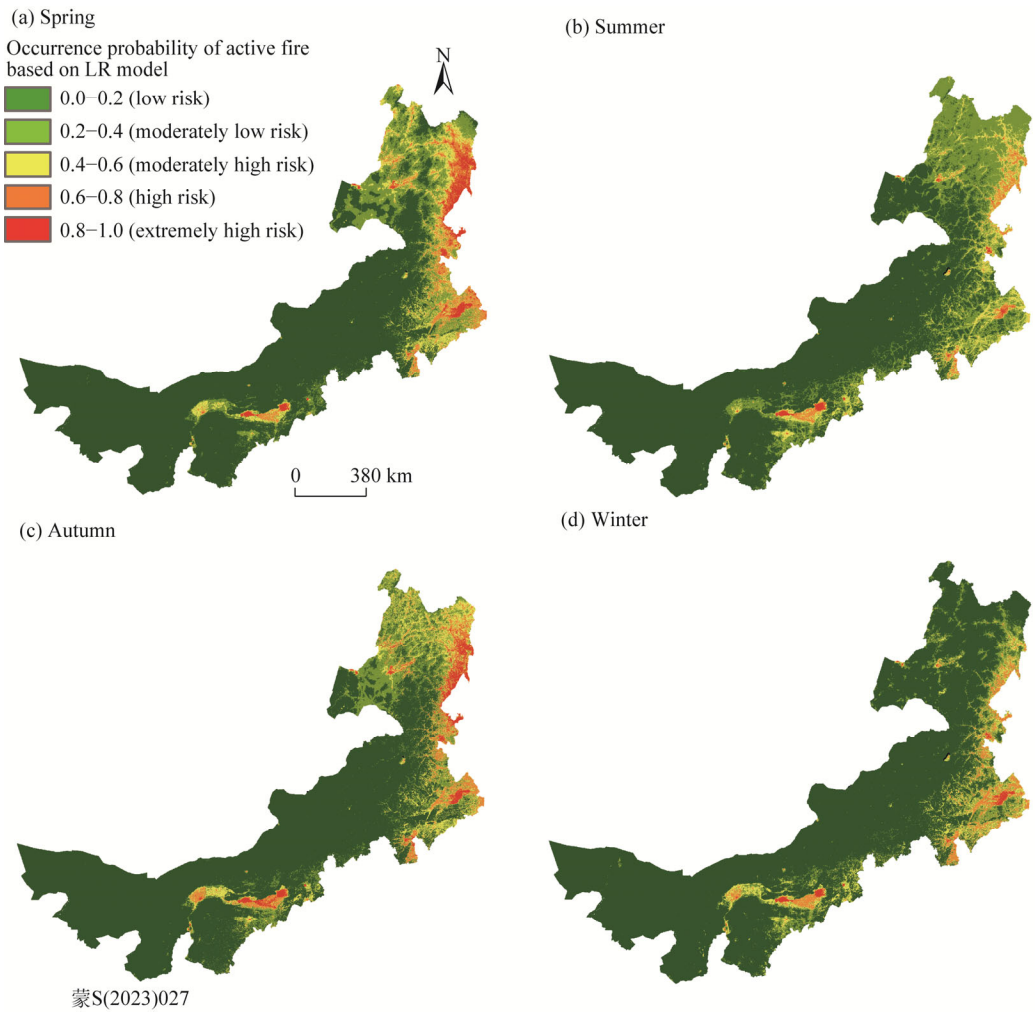

Fig. S2 Spatial distribution of fire risk level based on LR model at the seasonal scale. (a), spring; (b), summer; (c), autumn; (d), winter.

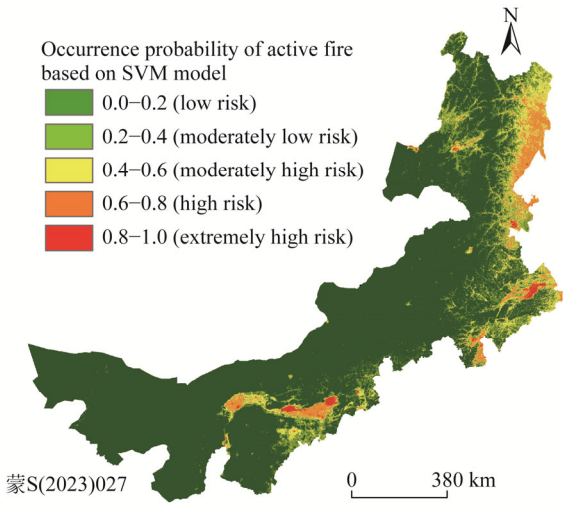

Fig. S3 Spatial distribution of fire risk level based on support vector machine (SVM) model from 2000 to 2022

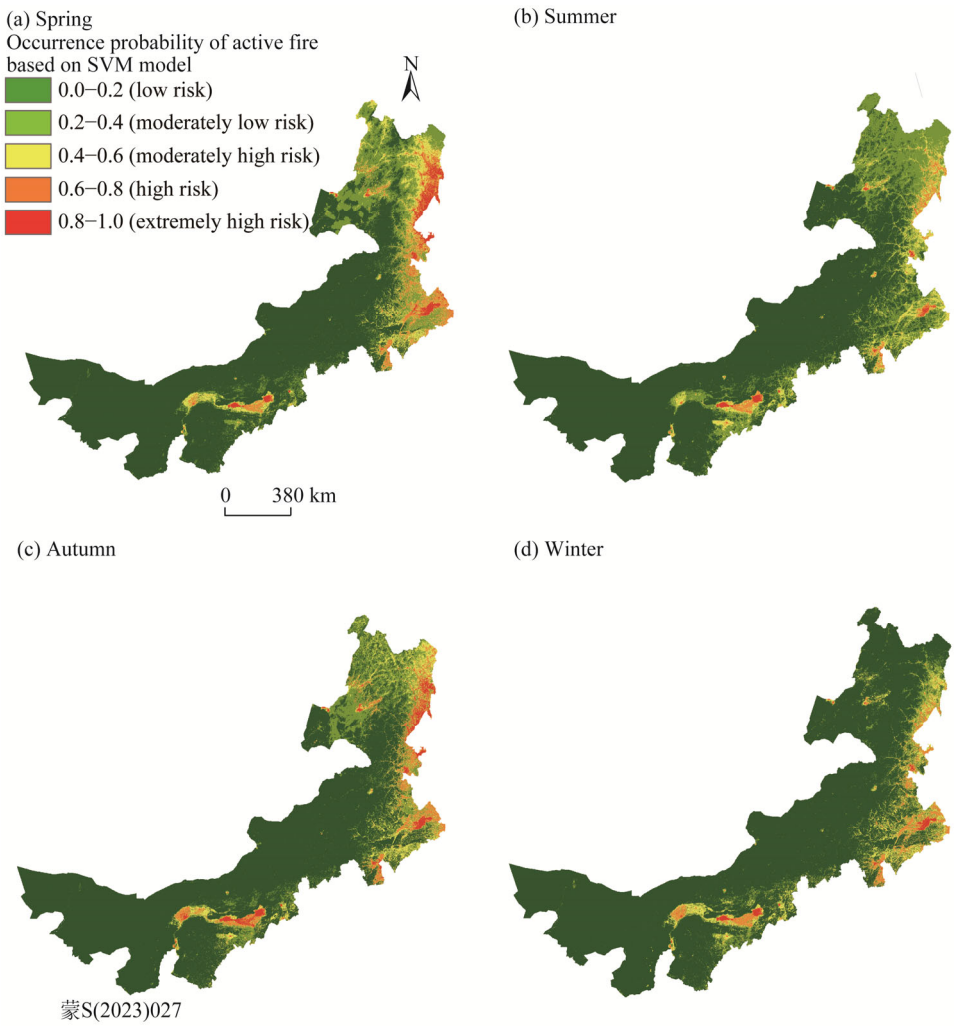

Fig. S4 Spatial distribution of fire risk level based on SVM model at the seasonal scale. (a), spring; (b), summer; (c), autumn; (d), winter.

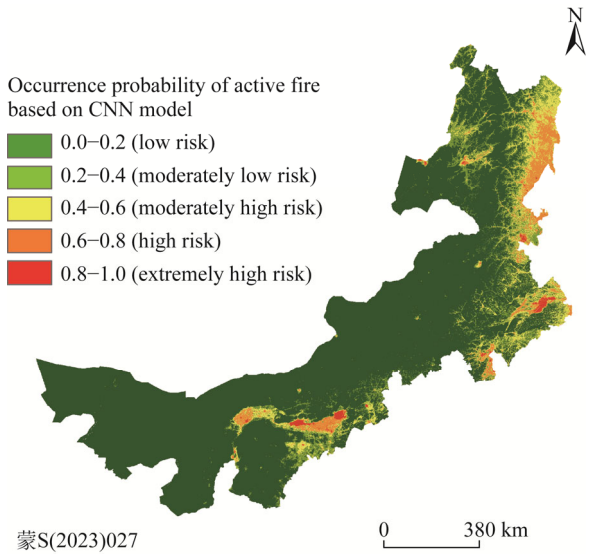

Fig. S5 Spatial distribution of fire risk level based on convolutional neural network (CNN) model from 2000 to 2022

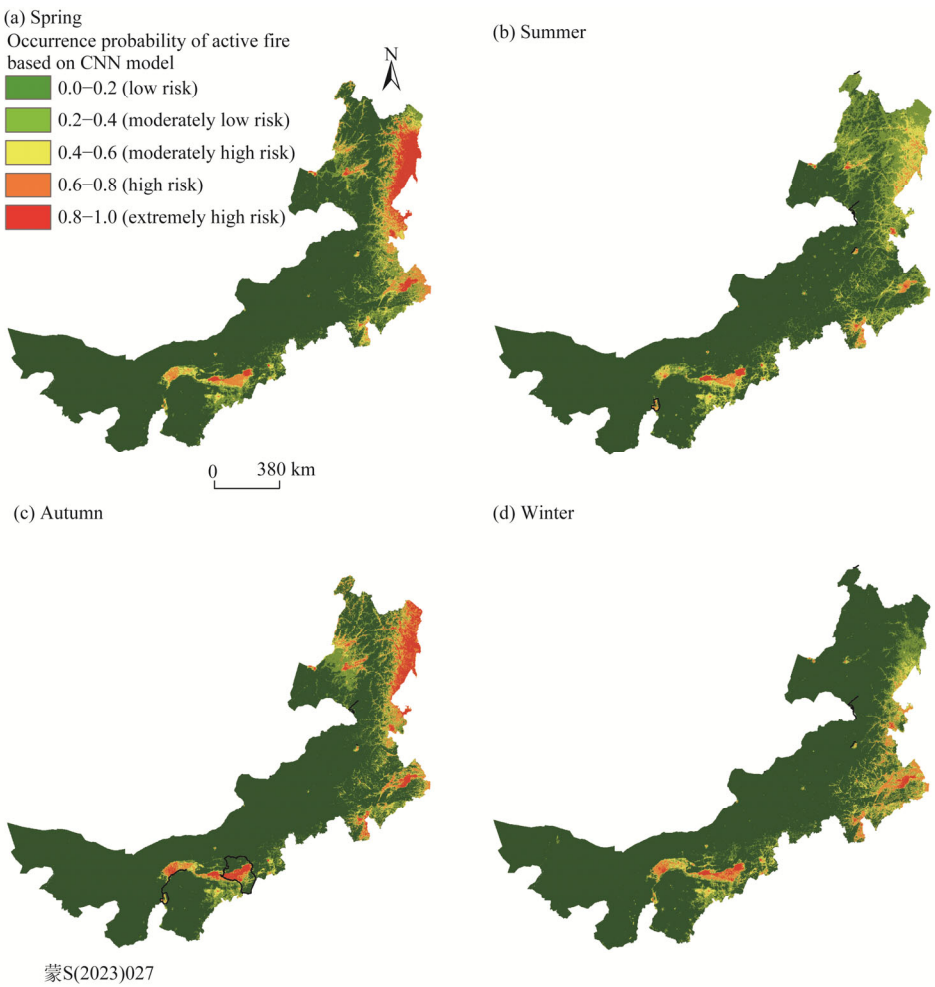

Fig. S6 Spatial distribution of fire risk level based on CNN model at the seasonal scale. (a), spring; (b), summer; (c), autumn; (d), winter.